Optics Letters

Gouy phase shift measurement using interferometric second-harmonic generation

Stéphane Bancelin,[1] Jarno N. Van der Kolk,[2] Andrew S. Quigley,[3] Maxime Pinsard,[1] Samuel P. Veres,[4] Laurent Kreplak,[3] Lora Ramunno,[2] and François Légaré[1,*]

[1]Institut National de la Recherche Scientifique, Centre Energie Matériaux et Télécommunications (INRS-EMT), Université du Québec, 1650 Boulevard Lionel Boulet, Varennes, Québec J3X 1S2, Canada
[2]Department of Physics and Centre for Research in Photonics, University of Ottawa, Ottawa, Ontario K1N 6N5, Canada
[3]Department of Physics and Atmospheric Science, Dalhousie University, 6310 Coburg Road, Halifax, Nova Scotia B3H 4R2, Canada
[4]Division of Engineering, Saint Mary's University, Halifax, Nova Scotia B3H 3C3, Canada
*Corresponding author: legare@emt.inrs.ca

Received 22 February 2018; revised 22 March 2018; accepted 22 March 2018; posted 23 March 2018 (Doc. ID 323152); published 17 April 2018

We report on a simple way to directly measure the Gouy phase shift of a strongly focused laser beam. This is accomplished by using a recent technique, namely, interferometric second-harmonic generation. We expect that this method will be of interest in a wide range of research fields, from high-harmonic and attosecond pulse generation to femtochemistry and nonlinear microscopy. © 2018 Optical Society of America

OCIS codes: (190.2620) Harmonic generation and mixing; (180.4315) Nonlinear microscopy; (190.4160) Multiharmonic generation; (190.4400) Nonlinear optics, materials.

https://doi.org/10.1364/OL.43.001958

It is well known that, across the focus of a freely propagating Gaussian beam, its phase experiences an additional π-shift compared to a plane wave. This is the so-called axial phase anomaly discovered by Gouy in 1890 [1]. This phase shift has significant consequences in nonlinear optics, since the observation of nonlinear processes requires high peak intensity, thus requiring focus of ultrashort laser pulses. Hence, determining and controlling the phase anomaly is crucial in many fields based on ultrafast light–matter interactions, e.g., THz generation [2,3], femtochemistry [4], and electron acceleration from nanostructures [5,6]. In particular, in attosecond science, few-cycle pulses are used to drive the strong-field processes, and this phase shift creates a spatially dependent carrier envelope phase (CEP) [7–9], which impacts how to design CEP-dependent strong-field experiments, such as the generation of isolated attosecond pulses [10,11]. In coherent nonlinear optical microscopy, the length of interaction is in the range of 1 μm; thus, one expects that phase matching should play no role. However, in processes such second- and third-harmonic generation (SHG and THG, respectively), the electric fields add coherently, and thus the Gouy phase shift strongly affects [12,13] the observed imaging contrast. As a consequence, in the last decade, there have been a number of experimental studies to monitor and map the spatial evolution of this phase anomaly [14–18].

In this Letter, we propose a direct technique to map the axial phase shift under tight focusing conditions using interferometric SHG (I-SHG) microscopy [19,20]. Since SHG is a phase-sensitive non-linear process, the axial phase change as the beam propagates through its focus can be extracted from the measurement of the phase of the signal generated by a point-like source at different positions within the focal volume. To that end, we spatially confined SHG over ∼100 nm using the field generated from a single collagen fibril, and measured its interference with a reference SHG beam generated before the microscope.

In this study, we used isolated collagen fibrils extracted and prepared following the protocol established in [21]. SHG imaging was performed using a custom-built laser-scanning microscope as described previously [22,23] (Fig. 1). In short, the laser source was a mode-locked Ti:Sapph oscillator (Tsunami pumped by a 12 W Millenia Pro laser, Spectra Physics) tuned at 810 nm and delivering ∼150 fs pulses at 80 MHz. A 5 cm focal lens was used to focus the laser on a 20-μm thick beta-barium borate (BBO) crystal ($\theta = 29.2°$, Eskma Optics) to generate a reference SHG beam whose

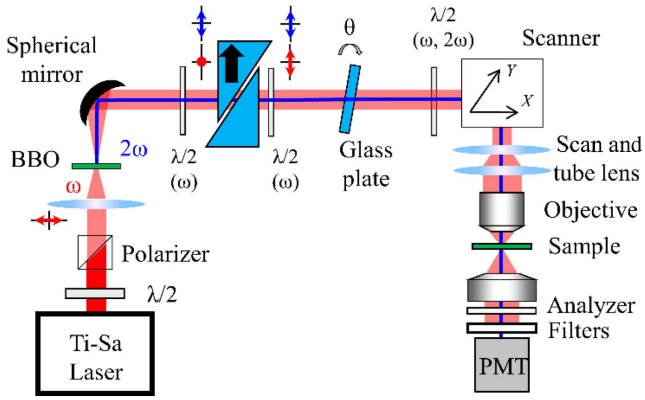


Fig. 1. Schematic of the I-SHG microscope.

Corrected 18 April 2018

intensity was adjusted by moving the crystal closer or farther from the lens focal point. Both the excitation beam (810 nm) and the reference SHG beam (405 nm) were collimated using a metallic spherical mirror. Two calcite wedges were inserted between two half-waveplates at 810 nm and full-waveplates at 405 nm, to introduce a controlled negative delay between the two beams that pre-compensate for the dispersion introduced by all the following optical elements. A 1.5 mm thick BK7 window, placed on a rotating mount, was used to control the phase between the reference and the excitation beam. A last half-wave plate (at 405 nm and 810 nm) was used to adjust the incident linear polarization before entering the microscope. The microscope was built on a telecentric scanner (TillPhotonics GmbH), and the beam was re-sized to overfill the back aperture of a water-dipping objective (Olympus, UplanSApo 40×W3/340, NA 1.1). Mechanical and piezoelectric motors, for coarse and fine adjustments, respectively, were used to vertically move the objective, allowing the acquisition of z-stacks. Signals were collected in the forward direction using a condenser [numerical aperture (NA) 0.55] and detected on a photomultiplier tube (PMT—R6357, Hamamatsu Photonics, Japan) set at 900 V using appropriate spectral filters (two FF01-720/SP-25 and a FF01-405/10, Semrock). Finally, an analyzer was placed just in front of the PMT, and set parallel to the collagen fibril observed. Scanning and signal acquisition were synchronized using a custom-written LabVIEW software and a multichannel I/O board (National Instruments).

20 μm × 40 μm images were recorded in the forward direction, in ∼2 s, using 20 μs pixel dwell time and 100 nm pixel size in order to oversample the fibril structure. The average power on the sample was adjusted to 30 mW, corresponding to 0.4 nJ/pulse. Raw data visualization was performed with ImageJ (NIH) and image processing was performed with MATLAB (The MathWorks) and Origin 10 (OriginLab).

The I-SHG technique aims at retrieving the relative phase of the SHG signal in the sample by measuring its interference with the reference SHG beam (for a complete description of the method, see [19,20]). The intensity measured on the PMT is given by

$$I(\varphi_{\mathrm{ref}}) = I_{\mathrm{ref}} + I_{\mathrm{samp}} + 2\sqrt{I_{\mathrm{ref}} I_{\mathrm{samp}}}\cos(\varphi_{\mathrm{samp}} - \varphi_{\mathrm{ref}}), \quad \textbf{(1)}$$

where φ_{ref} and I_{ref} (respectively, φ_{samp} and I_{samp}) stand for the phase and the intensity of the reference (respectively, sample) SHG beams. The reference phase can be adjusted by rotating the glass window. The relationship between φ_{ref} and the glass-window angle was calibrated using a 350 μm thick y-cut quartz plate as a sample, obtaining the typical interferometric pattern described by Stolle *et al.* [24]. As only the relative phase is relevant here, the zero value for the reference phase was assigned arbitrarily.

This calibration allows, when looking at a collagen fibril, to introduce a control phase shift between the two SHG beams. To isolate the interferometric term, we computed the difference between two raw images acquired with a π phase shift in φ_{ref}:

$$I(\varphi_{\mathrm{ref}}) - I(\varphi_{\mathrm{ref}} + \pi) = 4\sqrt{I_{\mathrm{ref}} I_{\mathrm{samp}}}\cos(\varphi_{\mathrm{samp}} - \varphi_{\mathrm{ref}}). \quad \textbf{(2)}$$

The acquisition of 12 pairs of images, with reference phase varying from 0° to 330° by 30° phase steps and fitting with Eq. (2), allows interpolation of the amplitude and relative phase of the interferometric contrast. For every pixel, we determine the reference phase corresponding to the maximum amplitude, which provides an image of the relative phase in the sample.

Note that the use of a laser-scanning system to scan the incident angle of the beams on the back pupil of the objective led to a change in the optical path, introducing a gradual phase shifting from the center of the interferometric pattern. While this could be calibrated and compensated [25], we choose here to limit our region of interest (ROI) to the very center of the field of view (20 μm × 40 μm).

Using I-SHG microscopy, we measured the phase of the SHG signal from isolated collagen fibrils. The excitation beam is propagating along the *z* axis, and the fibril is lying in the focal plane [*xy* plane, see Fig. 2(a)]. A phase histogram with a single narrow peak corresponds to the phase of the excitation beam [see Eq. (2)]. Since the diameter of collagen fibrils (10–500 nm) [26,27] is commonly well below the axial length of the point spread function (∼1 μm in these conditions), a single fibril acts as a point source. Therefore, acquiring a z-stack of a single collagen fibril is equivalent to scanning a point source within the focal volume, allowing us to probe the phase variation within the focal spot.

Figure 2 displays the Gaussian fit of the phase histogram for five different fibril axial positions within the focal spot. The lateral shift observed in the peak value at increasing depth

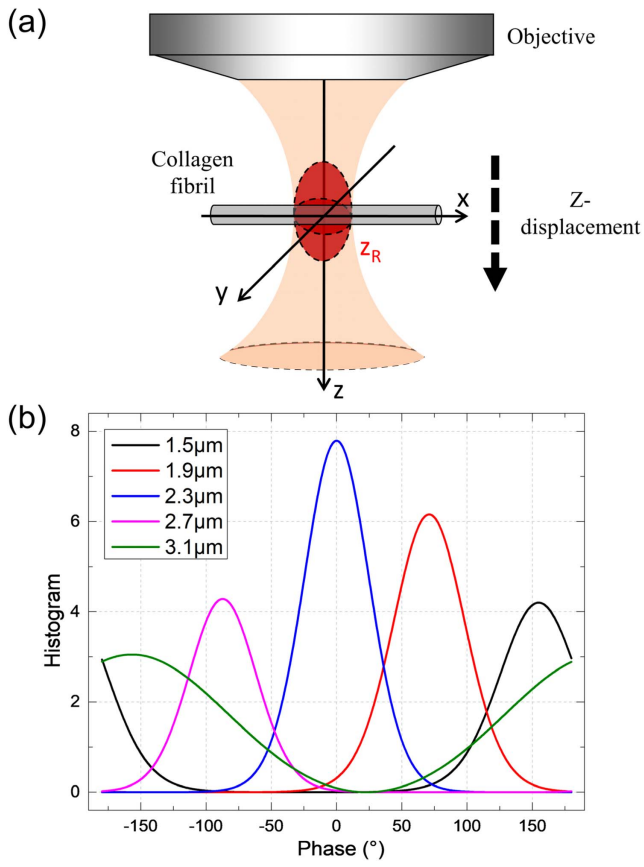


Fig. 2. (a) Schematic of the collagen fibril under laser excitation. (b) Gaussian fitting of the phase histogram measured in the same collagen fibril at different positions within the focal volume. The shift in the peak value reveals the variation of the phase of the excitation beam with focus position.

(Fig. 2) reveals the variation of the phase of the excitation beam with focus position, the so-called Gouy phase shift. Note that the absolute position of the peak is not relevant, as it depends on the choice of the zero reference phase. However, since this zero is defined during the calibration and is kept constant through all experiments, it allows extraction of the variation of phase while adjusting the depth of focus. Therefore, as a convention, we set the origin of the phase at the peak value obtained when the fibril is at the focus of the objective, indicated by the maximal intensity value in the z-stack. In addition, the variation of the peak width observable in Fig. 2 results from the decrease of the SHG signal when the collagen fibril is out of focus, which reduces the signal-to-noise ratio and therefore the accuracy of the phase peak determination.

To accurately measure the Gouy phase shift we displaced the focal volume over 6 μm by 0.15 μm steps and acquired both SHG and I-SHG images at each step. Figure 3 displays the intensity of SHG signal (red squares—top panel) as a function of fibril position within the focal volume together with the evolution of the phase (red squares—bottom panel). It is worth noting that we observe a 2π phase step, since the SHG signal results from the square of the excitation electric field, and therefore the phase shift of the SHG signal is double the one of the excitation beam.

As a first approximation, the phase exhibits the classical arctangent-like behavior of the Gouy phase shift:

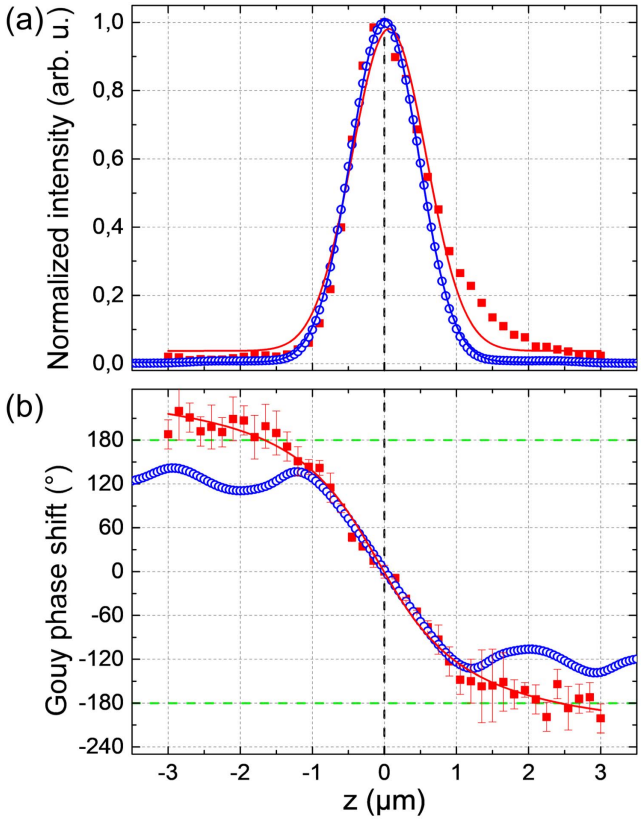


Fig. 3. (a) Intensity profile and (b) Gouy phase shift as a function of fibril position within the focal spot. Red squares indicate experimental measurements, and blue circles represent numerical simulations. Plane lines represent Gaussian fitting in (a) or fitting along Eq. (3) in (b).

$$\varphi_{\text{Gouy}} = -2\arctan\left(\frac{z}{z_R}\right), \tag{3}$$

where z_R is the Rayleigh range of the excitation beam. Fitting the Gouy phase shift using Eq. (3), we obtain a Rayleigh range of 930 ± 80 nm, which is consistent with the one extracted from the intensity profile 1030 ± 40 nm. Note that this corresponds to the theoretical Rayleigh range obtained with a 1.0 NA objective (934 nm), which might indicate a slight under-filling of the back aperture of the objective or result from spherical aberrations.

However, since we are using a tightly focused beam in these experiments, Eq. (3) is not valid anymore, and one has to consider the case of a vector field. In this case, the Gouy phase anomaly is defined as the difference between the actual phase of the wave and the one of a spherical wave [28,29]. Furthermore, in the case of a vector field, the polarization of the beam needs to be considered [30].

To calculate the Gouy phase shift of a tightly focused beam, we used numerical simulations. These simulations were performed by illuminating a 110 nm diameter cylinder, lying in the x direction, with a tightly focused beam [30–32] with a 1.0 NA in a $n = 1.33$ medium, propagating in the z direction. The induced nonlinear polarization (P) is then calculated as

$$\vec{P} = \chi^{(2)} : \vec{E}\,\vec{E}\,, \tag{4}$$

where $\chi^{(2)}$ is the second-order nonlinear susceptibility tensor for collagen fibrils [33] and E the incident electric field. The far-field emitted electric fields are then calculated using the Green's function approach as in [19], and we determine both the intensity and the phase (blue circles—top and bottom panels, respectively). Note that in the simulations, the Gouy phase shift actually does go from −180° to +180° at longer length scale.

In the case of a vector field, one would expect that the Gouy phase shift depends upon the three incident P components, as in [30]. In our simulations, this dependency is accounted for through the tensor nature of $\chi^{(2)}$. This corresponds to our experimental conditions, where the SHG signal is a mix of the contributions of the three incident components of P due to tight focusing.

In conclusion, we have presented a simple technique to measure the Gouy phase anomaly of strongly focused short pulses by means of I-SHG microscopy. The technique allows an accurate measurement of the smooth evolution of the phase through the focus. We expect that this method will be of interest in a wide range of research fields, from high-harmonic and attosecond pulse generation to femtochemistry and nonlinear microscopy.

Funding. Canada Foundation for Innovation (CFI); Natural Sciences and Engineering Research Council of Canada (NSERC); Fonds de Recherche du Québec—Nature et Technologies (FRQNT).

REFERENCES

1. L. G. Gouy, Compt. Rendue Acad. Sci. **110**, 1251 (1890).
2. P. Klarskov, A. C. Strikwerda, K. Iwaszczuk, and P. U. Jepsen, New J. Phys. **15**, 075012 (2013).
3. Y. Bai, L. Song, R. Xu, C. Li, P. Liu, Z. Zeng, Z. Zhang, H. Lu, R. Li, and X. Xu, Phys. Rev. Lett. **108**, 255004 (2012).

4. R. J. Gordon and V. J. Barge, J. Chem. Phys. **127**, 204302 (2007).
5. M. Krüger, M. Schenk, and P. Hommelhoff, Nature **475**, 78 (2011).
6. S. Zherebtsov, T. Fennel, J. Plenge, E. Antonsson, I. Znakovskaya, A. Wirth, O. Herrwerth, F. Süßmann, C. Peltz, I. Ahmad, S. A. Trushin, V. Pervak, S. Karsch, M. J. J. Vrakking, B. Langer, C. Graf, M. I. Stockman, F. Krausz, E. Rühl, and M. F. Kling, Nat. Phys. **7**, 656 (2011).
7. F. Lindner, G. G. Paulus, H. Walther, A. Baltuška, E. Goulielmakis, M. Lezius, and F. Krausz, Phys. Rev. Lett. **92**, 113001 (2004).
8. T. Tritschler, K. D. Hof, M. W. Klein, and M. Wegener, Opt. Lett. **30**, 753 (2005).
9. Y. H. Zhou, H. B. Jiang, and Q. H. Gong, Chin. Phys. Lett. **23**, 110 (2006).
10. M. Hentschel, R. Kienberger, Ch. Spielmann, G. A. Reider, N. Milosevic, T. Brabec, P. Corkum, U. Heinzmann, M. Drescher, and F. Krausz, Nature **414**, 509 (2001).
11. R. Kienberger, E. Goulielmakis, M. Uiberacker, A. Baltuška, V. Yakovlev, F. Bammer, A. Scrinzi, Th. Westerwalbesloh, U. Kleineberg, U. Heinzmann, M. Drescher, and F. Krausz, Nature **427**, 817 (2004).
12. L. Moreaux, O. Sandre, S. Charpak, M. Blanchard-Desce, and J. Mertz, Biophys. J. **80**, 1568 (2001).
13. J. Mertz and L. Moreaux, Opt. Commun. **196**, 325 (2001).
14. J. H. Chow, G. de Vine, M. B. Gray, and D. E. McClelland, Opt. Lett. **29**, 2339 (2004).
15. H. Kandpal, S. Raman, and R. Mehrotra, Opt. Lasers Eng. **45**, 249 (2007).
16. Z. Wang, Z. Zeng, R. Li, and Z. Xu, Chin. Opt. Lett. **5**, S183 (2007).
17. P. Bon, B. Rolly, N. Bonod, J. Wenger, B. Stout, S. Monneret, and H. Rigneault, Opt. Lett. **37**, 3531 (2012).
18. K. J. Kaltenecker, J. C. König-Otto, M. Mittendorff, S. Winnerl, H. Schneider, M. Helm, H. Helm, M. Walther, and B. M. Fischer, Optica **3**, 35 (2016).
19. M. Rivard, K. Popov, C.-A. Couture, M. Laliberté, A. Bertrand-Grenier, F. Martin, H. Pépin, C. P. Pfeffer, C. Brown, L. Ramunno, and F. Légaré, J. Biophoton. **7**, 638 (2013).
20. C.-A. Couture, S. Bancelin, J. Van der Kolk, K. Popov, M. Rivard, K. Légaré, G. Martel, H. Richard, C. Brown, S. Laverty, L. Ramunno, and F. Légaré, Biophys. J. **109**, 2501 (2015).
21. A. Quigley, S. Bancelin, D. Deska-Gauthier, F. Légaré, L. Kreplak, and S. P. Veres, Sci. Rep. **8**, 4409 (2018).
22. M.-A. Houle, C.-A. Couture, S. Bancelin, J. Van der Kolk, E. Auger, C. Brown, K. Popov, L. Ramunno, and F. Légaré, J. Biophoton. **8**, 993 (2015).
23. S. Bancelin, C.-A. Couture, M. Pinsard, M. Rivard, P. Drapeau, and F. Légaré, Sci. Rep. **7**, 6758 (2017).
24. R. Stolle, G. Marowsky, E. Schwarzberg, and G. Berkovic, Appl. Phys. B **63**, 491 (1996).
25. S. Bancelin, C.-A. Couture, K. Légaré, M. Pinsard, M. Rivard, C. Brown, and F. Légaré, Biomed. Opt. Express **7**, 399 (2016).
26. K. E. Kadler, C. Baldock, J. Bella, and R. P. Boot-Handford, J. Cell Sci. **120**, 1955 (2007).
27. D. J. S. Hulmes, J. Struct. Biol. **137**, 2 (2002).
28. M. Born and E. Wolf, *Principles of Optics*, 7th ed. (Cambridge University, 1999).
29. T. D. Visser and E. Wolf, Opt. Commun. **283**, 3371 (2010).
30. P. Xiaoyan, T. D. Visser, and E. Wolf, Opt. Commun. **284**, 5517 (2011).
31. J.-X. Cheng, A. Volkmer, and X. S. Xie, J. Opt. Soc. Am. B **19**, 1363 (2002).
32. B. Richards and E. Wolf, Proc. R. Soc. London A **253**, 358 (1959).
33. A. Erikson, J. Ortegren, T. Hompland, C. de Lange Davies, and M. Lindgren, J. Biomed. Opt. **12**, 044002 (2007).